ACS OMEGA

http://pubs.acs.org/journal/acsodf

Article

Superiority of an Asymmetric Perylene Diimide in Terms of Hydrosolubility, G-Quadruplex Binding, Cellular Uptake, and Telomerase Inhibition in Prostate Cancer Cells

Ratasark Summart, Pak Thaichana, Jutharat Supan, Puttinan Meepowpan, T. Randall Lee, and Wirote Tuntiwechapikul*

Cite This: *ACS Omega* 2020, 5, 29733−29745

Read Online

ACCESS | Metrics & More | Article Recommendations | Supporting Information

ABSTRACT: Perylene diimide (PDI) derivatives have been studied as G-quadruplex ligands that suppress telomerase activity by facilitating G-quadruplex formation of telomeric DNA and the *hTERT* promoter. PIPER, the prototypical PDI, reduces telomerase activity in lung and prostate cancer cells, leading to telomere shortening and cellular senescence of these cells. However, PIPER suffers from poor hydrosolubility and the propensity to aggregate at neutral pH. In this report, we synthesized a new asymmetric PDI, aPDI-PHis, which maintains one *N*-ethyl piperidine side chain of PIPER and has histidine as another side chain. The results show that aPDI-PHis is superior to its symmetric counterparts, PIPER and PDI-His, in terms of hydrosolubility, G-quadruplex binding, cellular uptake, and telomerase inhibition in prostate cancer cells. These results suggest that one *N*-ethyl piperidine side chain of PDI is sufficient for G-quadruplex binding, while another side chain can be tuned to elicit desirable properties. These findings might lead to better PDIs for use as anticancer drugs.

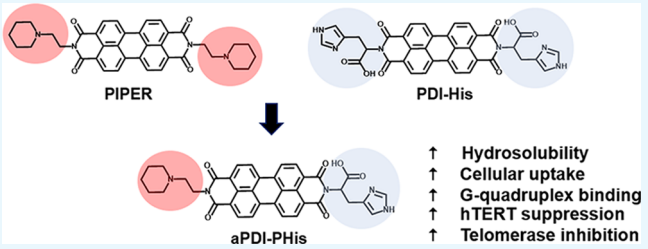

INTRODUCTION

Telomerase is a ribonucleoprotein enzyme that is vital for the immortality characteristic of most cancers.[1] It is an attractive target for anticancer therapy due to the lack of active telomerase in most normal somatic cells, preventing them from the unwanted side effects associated with most conventional anticancer drugs.[2] Telomerase maintains the length of telomeres in human cancer cells by progressive addition of the telomeric repeat sequence (TTAGGG) to the 3′-end of telomeric DNA, thereby preventing the cell from replicative senescence typically observed in normal somatic cells.[1] A telomerase-specific inhibitor allows cancer cells to succumb to the same replicative senescence as normal cells, albeit faster due to their rapid cell division and shorter telomeres than in normal tissues.[3,4]

Prostate cancer is expected to be the most diagnosed cancer among men in the United States in 2020.[5] Prostate cancers maintain their telomeres predominantly via telomerase; thereby, they are good candidates for telomerase inhibition therapy. Furthermore, prostate cancer stem cells, which are responsible for cancer relapse, have short telomeres, and exhibit vigorous telomerase activity.[6] Thus, telomerase inhibition can affect both tumor cells and cancer stem cells. Also, prostate cancer grows relatively slowly compared to other types of cancers, often with no adverse effects for years.[7] As a result, active surveillance is now recommended for patients with low-grade and early-stage prostate cancer as an alternative to surgical and medical treatments that are associated with unwanted side effects.[8] These patients are likely to benefit from telomerase inhibition by slowing the progress of prostate cancer.

G-quadruplexes (G4s) are secondary nucleic acid structures formed from a stack of G-tetrads, which are planar ring structures constructed from reverse Hoogsteen hydrogen bonding among four guanines.[9] Small molecules that facilitate and stabilize G4 structures represent the most widely studied telomerase inhibitors.[10,11] These G4 ligands exert their telomerase inhibition through intramolecular G4 formations of telomeric DNA and the *hTERT* promoter.[10−13] The quadruplex formation at the 3′-overhang of the telomere prevents telomerase from accessing its substrate and thereby inhibits its activity.[10−12] In contrast, quadruplex formation within the *hTERT* promoter suppresses the gene expression of the hTERT protein, the catalytic subunit of telomerase, leading to subdued telomerase activity in cancer cells.[12] Notably, when cancer cells were treated with G4 ligands, the cells displayed

Received: July 22, 2020
Accepted: November 5, 2020
Published: November 12, 2020

https://dx.doi.org/10.1021/acsomega.0c03505
ACS Omega 2020, 5, 29733−29745

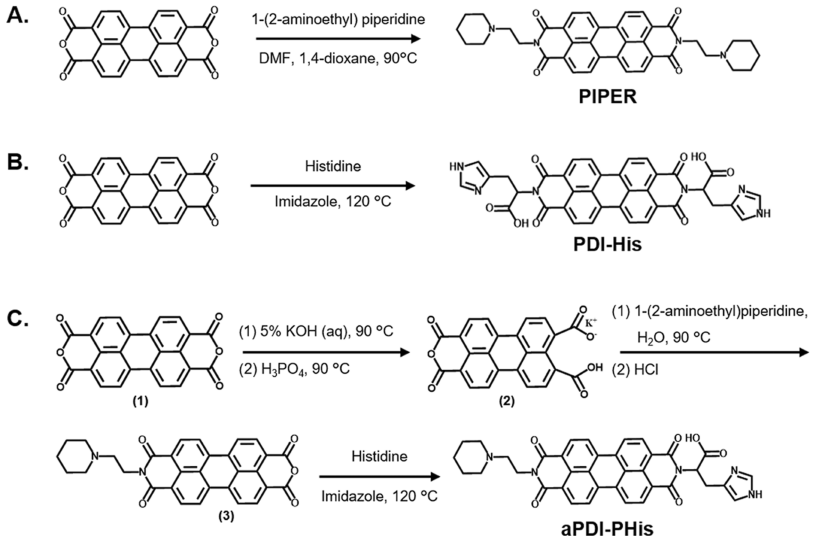

Figure 1. Synthetic schemes of (A) PIPER, (B) PDI-His, and (C) aPDI-PHis.

telomere shortening after successive rounds of cell division, which eventually led to cellular senescence or apoptosis.[12,14,15]

Perylene diimide (PDI) derivatives are widely studied as G4 ligands and telomerase inhibitors.[16] The aromatic core of perylene binds to the outer G-tetrad of the G4 via $\pi-\pi$ interactions, while the hydrophilic side chains interact with the DNA grooves.[16] PIPER, the prototypical PDI, was shown to suppress telomerase and induce telomere shortening in lung and prostate cancer cells.[12,17] However, PIPER is well known for its self-aggregation at neutral to basic pH,[18] which might be problematic from a pharmaceutical perspective. Many strategies have been employed to increase the hydrosolubility and yet maintain G4 binding selectivity of PDIs; these include side-chain and bay-area modifications.[16,19,20] Even though the addition of one or more side chains in the bay area of PDIs could diminish self-aggregation by decreasing the planarity of the perylene core, it would also reduce the stacking on the outer G-quartet of G4 DNAs.[16,20] Besides, the addition of the hydrophilic side chain(s) would significantly increase the molecular weight and would likely influence cellular uptake. Side-chain modifications of PDIs are mostly symmetric, and the side chains are limited to cationic moieties because the electrostatic interactions with the sugar−phosphate backbone at the G4 groove are deemed to be essential.[16] However, we believe that only one cationic side chain is essential for G4 binding based on our experience with perylene monoimide (PMI) derivatives.[21] Therefore, a different side chain could be attached to PDIs to achieve desirable properties but still maintain their G4 DNA binding.

In this study, we designed and synthesized an asymmetric PDI, aPDI-PHis. We hypothesized that it would be more soluble than PIPER but still able to bind G4 DNA selectively. This compound has one piperidine side chain and one histidine side chain (Figure 1C). The piperidine side chain is identical to those in PIPER, which we felt would enable aPDI-PHis to bind to G4 DNA. We chose histidine as the other side chain because it is a natural amino acid with a branched structure of two opposing charged moieties: the carboxylic group and the imidazole ring. At physiological pH, the carboxylic group is negatively charged, which would enhance its hydrosolubility, while the imidazole ring is mostly neutral. Under mildly acidic conditions, the imidazole group (with $pK_a \cong 6$) is somewhat protonated, which partially counterbalances the carboxylic group's negative charge. Considering that the cancer extracellular microenvironment is mildly acidic, the histidine side chain's balanced charges might aid cellular uptake of this compound to cancer cells.[22] Herein, we report the synthesis of aPDI-PHis and its symmetric counterparts: PIPER and PDI-His. We investigated their UV−vis absorption, fluorescence emission, hydrosolubility, octanol/water distribution, cellular uptake, and G4 binding selectivity at three physiologically relevant pHs. We also investigated their acute cytotoxicity, *hTERT* gene suppression, and telomerase inhibition in two prostate cancer cell lines.

RESULTS AND DISCUSSION

Synthesis of Perylene Diimide Derivatives. The syntheses of PIPER and PDI-His followed the protocols from the literature that we previously published.[23] In these syntheses, perylene-3,4,9,10-tetracarboxylic dianhydride (PTCDA) was refluxed with 1-(2-aminoethyl)piperidine or histidine in an appropriate solvent to form PIPER or PDI-His, respectively (Figure 1A,B). The synthesis of aPDI-PHis followed a synthetic strategy described by Williams (Figure 1C).[24] First, both anhydride rings of PTCDA (**1**) were hydrolyzed by 5% KOH in water. Then, one anhydride ring was reformed to give the perylene monoimide-monoanhydride (**2**) by a dropwise addition of H_3PO_4 until the pH of the mixture was between 4.5 and 5.5. The 1-(2-aminoethyl)piperidine side chain was then attached to (**2**) through the anhydride group by refluxing the reaction mixture at 90 °C for 3 h. The two remaining carboxylic groups were dehydrated to form an anhydride ring of (**3**) by the addition of 2 M HCl. Finally, the histidine side chain was attached to (**3**) by refluxing the reaction mixture in imidazole at 120 °C for 3 h to obtain the reddish-pink aPDI-PHis (**4**). The detailed synthesis and characterization data of these compounds are provided in Section S1 and Figures S1.1−1.3, Supporting Information.

Photoproperty of the Perylenes. Hydrosoluble perylene diimide derivatives have been studied as fluorescent dyes for environmental and biological analyses due to their strong fluorescence emission and high photostability.[25,26] These derivatives have also been employed as fluorescent probes

https://dx.doi.org/10.1021/acsomega.0c03505
ACS Omega 2020, 5, 29733−29745

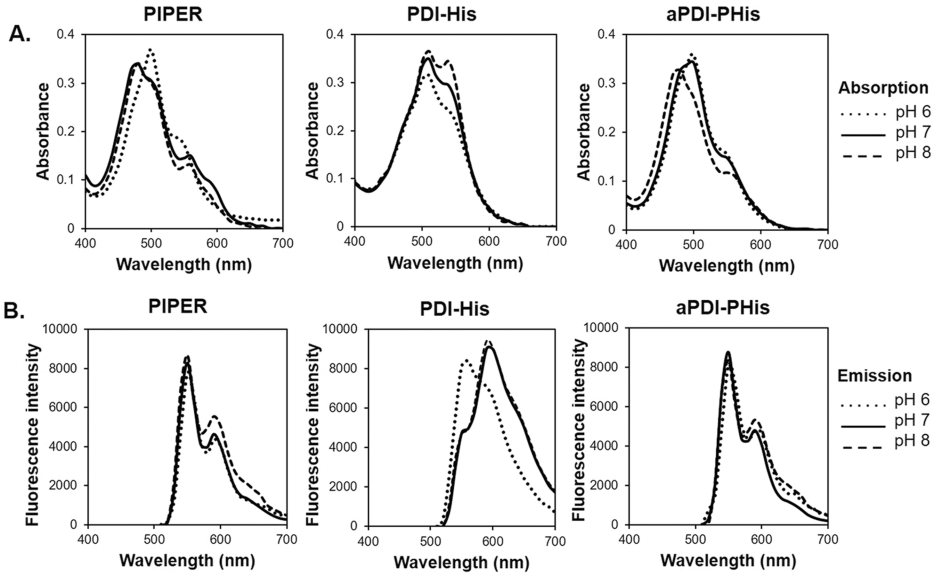

Figure 2. Visible light absorption (A) and fluorescence emission (B) spectra of the perylenes. (A) The indicated PDI (40 μM) was suspended in 500 μL of 10 mM potassium phosphate buffer. The visible wavelengths between 400 and 700 nm were recorded using a spectrophotometer. (B) A 200 μL aliquot of each PDI (40 μM) in 10 mM potassium phosphate buffer was dispensed into a 96-well microplate. The fluorescence spectra between 520 and 700 nm were recorded using a Synergy H4 hybrid microplate reader with excitation wavelength at 480 nm.

for cell and organelle imaging.[27,28] In the present study, we investigated the photoproperty of our perylene derivatives at physiologically relevant pHs. The test compound (40 μM) was dissolved in 500 μL of 10 mM potassium phosphate buffer (pH 6−8). The visible wavelengths between 400 and 700 nm were recorded using a UV-1800 double-beam spectrophotometer (Shimadzu Scientific). As shown in Figure 2A, PIPER exhibits a maximum absorption wavelength (λ_{max}) of 480 nm at pH 7 and pH 8, but the λ_{max} red-shifts to 500 nm at pH 6. The λ_{max} of PDI-His (510 nm) is invariant at all three pHs. However, there is an increase in the area under the absorption spectra and a rise of the secondary peak at 540 nm with the increasing pH. For aPDI-PHis, the λ_{max} is 500 nm at pH 6 and 7, but the λ_{max} blue-shifts to 480 nm at pH 8.

For fluorescence emission of our PDIs, 200 μL of each compound [40 μM in 10 mM potassium phosphate buffer (pH 6−8)] was dispensed into a 96-well microplate, and the fluorescence spectra between 520 and 700 nm were recorded using a Synergy H4 hybrid microplate reader (BioTek Instruments) with excitation wavelength at 480 nm. As shown in Figure 2B, PIPER and aPDI-PHis exhibit a maximum fluorescence emission of 550 nm and a secondary peak at 600 nm. The spectra are invariant at all three pHs. On the other hand, PDI-His shows a significant blue shift in fluorescence emission (560 nm) at pH 6, compared with emissions at pH 7 and 8 (590 nm).

The pH-related changes in the optical properties of our PDIs probably arise from several factors such as the ionic states, the distribution of microspecies, and the aggregation of the compounds. The ionic state can shift the absorption spectrum and change the molar absorption coefficient of a compound, which will affect the area under the curve. The percentages of microspecies distribution in the solution at a certain pH can also affect the spectrum. Our PDIs exist in three forms of microspecies between pH 6 and 8, based on calculations using MarvinSketch software with the pK_a function (see Figures S2.1−S2.3 in the Supporting Information). The ionic states and the percentage of microspecies distribution alone cannot fully explain the subtle spectral changes at these three pHs. Moreover, perylene diimides are also known for their self-aggregation in aqueous solution, and our PDIs are no exceptions (see Figure 3 below). Aggregation of the

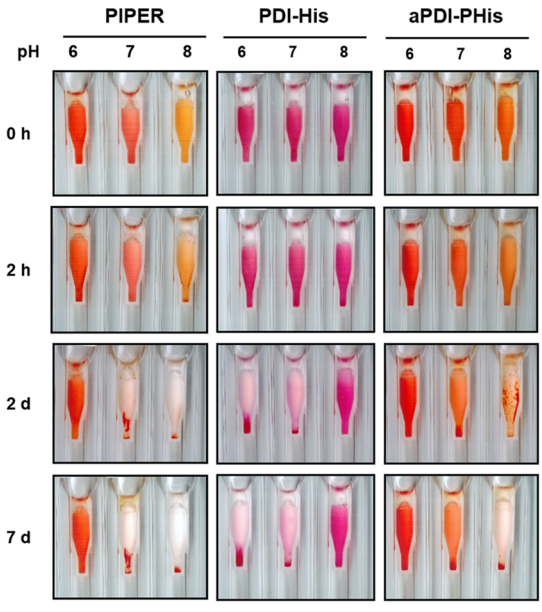

Figure 3. Hydrosolubility of the perylenes. Each cuvette contained 40 μM PDI in 10 mM potassium phosphate buffer (pH 6−8) in a total volume of 500 μL. The solubility and aggregation were observed and recorded using a camera for seven days.

compounds generally reduces the absorption intensity, although its full effect might not be prominent at measurement. With several factors in play, it is unwise to propose simple explanations for our optical results.

Hydrosolubility of the Perylenes. As mentioned earlier, we hypothesized that aPDI-PHis would be more hydrosoluble than PIPER at physiologically relevant pHs. To test the

https://dx.doi.org/10.1021/acsomega.0c03505
ACS Omega 2020, 5, 29733−29745

solubility of these three PDIs (PIPER, aPDI-PHis, or PDI-His), we dissolved each perylene (40 μM) in 10 mM potassium phosphate buffers (pH 6−8) and observed the solubility and precipitation of these compounds at various times up to seven days. As shown in Figure 3, all perylenes were homogeneously dispersed at all three pHs at time 0. As expected, PIPER, with its protonated piperidine side chains, remained soluble at pH 6 throughout the seven days. With increasing pH, the nonionized form of PIPER increases, and the compound completely aggregated at pH 7 and 8 after 2 days. In contrast, PDI-His remained soluble throughout the seven days at pH 8 but mostly aggregated at pH 6 and 7 after two days. At these three pHs, the two carboxylic groups of the histidine side chains of PDI-His are deprotonated and have negative charges. However, when the solution becomes more acidic, the imidazole rings ($pK_a \cong 6$) begin to protonate, and their positive charges counterbalance the negative charges of the carboxylic groups. Therefore, the compound starts to aggregate at pH 6 and 7. In contrast, aPDI-PHis seemed to incorporate the characteristics of both the piperidine side chain and the histidine side chain. It remained soluble at pH 6 and partially soluble at pH 7 after seven days. However, it started to aggregate at pH 8 on day 2 and completely precipitated on day 7. Based on these results, aPDI-PHis appears to have a broader range of solubility in aqueous solution than PIPER and PDI-His at these physiologically relevant pHs.

Octanol/Water Distribution of the Perylenes. Most drugs are absorbed through passive diffusion, which relies on the lipophilicity of the compounds. At the same time, they must be sufficiently hydrophilic to dissolve in an aqueous solution for transportation to the target site. In pharmaceutical sciences, the balance between hydrophilicity and lipophilicity is measured in two immiscible solvents, water and 1-octanol, in terms of the partition coefficient and the distribution coefficient.[29] In this study, we investigated the octanol/water distribution of the three perylenes at pH 6−8 following the OECD guidelines for testing chemicals no. 107 by the shake-flask method.[30] The test compound at the indicated concentration was dissolved in buffer-saturated 1-octanol before mixing with 10 mM phosphate buffer at the indicated pH. The bottles were then shaken vigorously for 15 min and centrifuged at 7000g for 10 min for phase separation. Figure 4 shows the octanol/water distribution of the perylenes after the phase separation. PIPER preferentially dissolves in water (lower layer) at pH 6, but it preferentially dissolves in octanol (upper layer) at pH 7 and 8. In contrast, PDI-His preferentially dissolves in water at pH 7 and 8. Interestingly, PDI-His aggregated at the interface of the two solvents at pH 6. In contrast, aPDI-PHis preferentially dissolves in octanol at all three pHs. We then calculated the $\log D_{o/w}$ based on absorbance measurements of a single liquid phase as previously described by Wattanasin et al.[31] The $\log D_{o/w}$ values of these perylenes at pH 6−8 are summarized in Table 1. The $\log D_{o/w}$ of PDI-His at pH 6 is nondeterminable due to the aggregation mentioned above.

From the previous hydrosolubility test, we found that both PIPER and aPDI-PHis dissolve well in an aqueous solution at pH 6. However, in this octanol/water distribution experiment, we found that aPDI-PHis dissolved in the octanol phase, while PIPER dissolved in the aqueous phase at pH 6. Therefore, it is likely that aPDI-PHis can diffuse through lipid bilayers better than PIPER when the environment is mildly acidic.

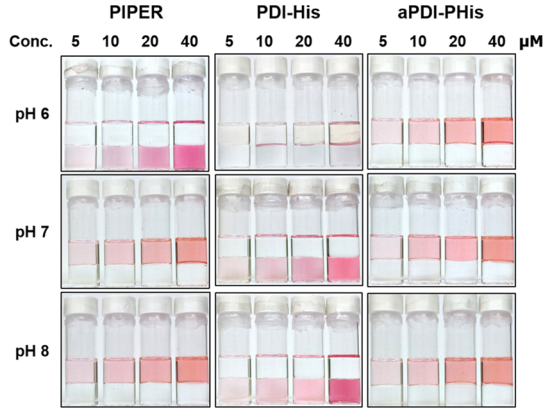

Figure 4. Distribution of the perylenes in octanol and water at various pHs. The test compound at the indicated concentration was first dissolved in 2 mL of buffer-saturated 1-octanol before mixing with 2 mL of 10 mM phosphate buffer at the indicated pH. The bottles were then shaken vigorously for 15 min and centrifuged at 7000g for 10 min for phase separation.

Table 1. Distribution Coefficients of the Perylenes[a]

compound	pH	$\log D_{o/w}$
PIPER	6.0	−2.23 ± 0.24
	7.0	2.10 ± 0.09
	8.0	2.03 ± 0.10
PDI-His	6.0	ND
	7.0	−2.22 ± 0.06
	8.0	−2.23 ± 0.06
aPDI-PHis	6.0	2.42 ± 0.18
	7.0	2.41 ± 0.18
	8.0	2.25 ± 0.07

[a]ND = nondeterminable.

Cellular Uptake of the Perylenes. To investigate the cellular uptake of the PDIs, we employed flow cytometry to measure the fluorescence intensity of these three compounds in PC3 and LNCaP prostate cancer cells and also in a human embryonic kidney cell line (HEK293). The cells were first seeded in pH-adjusted culture media (pH 6−8) at 37 °C for 24 h before they were treated with 0−16 μM of the indicated PDI for another 24 h. Cells were then analyzed by flow cytometry using Kaluza software program (Beckman Coulter). The fluorescence intensity distribution data are shown in Figure S3, Supporting Information. The bar graphs representing the results from three independent experiments are shown in Figure 5.

As shown in Figure 5A for PC3, 5B for LNCaP, and 5C for HEK293 cells, all three PDIs were uptaken into all three cell lines in a concentration-dependent manner within 24 h of incubation, showing that their concentrations did not reach the maximum absorption under these conditions. Moreover, these cell lines took up the three PDIs in a similar manner at all three pHs. In general, the cellular uptake of these PDIs is closely related to their solubility. At the pH where the PDIs dissolve more readily, the cellular uptake is greater. For example, aPDI-PHis is soluble in the order of pH 6 > pH 7 > pH 8, and the cellular uptake follows this order. On the other hand, PDI-His is soluble in the order of pH 8 > pH 7 > pH 6, and the cellular uptake follows this order as well. Interestingly, PDI-His is barely absorbed to all three cell lines at pH 6, the pH where PDI-His aggregated at the octanol/water interphase, as seen

https://dx.doi.org/10.1021/acsomega.0c03505
ACS Omega 2020, 5, 29733−29745

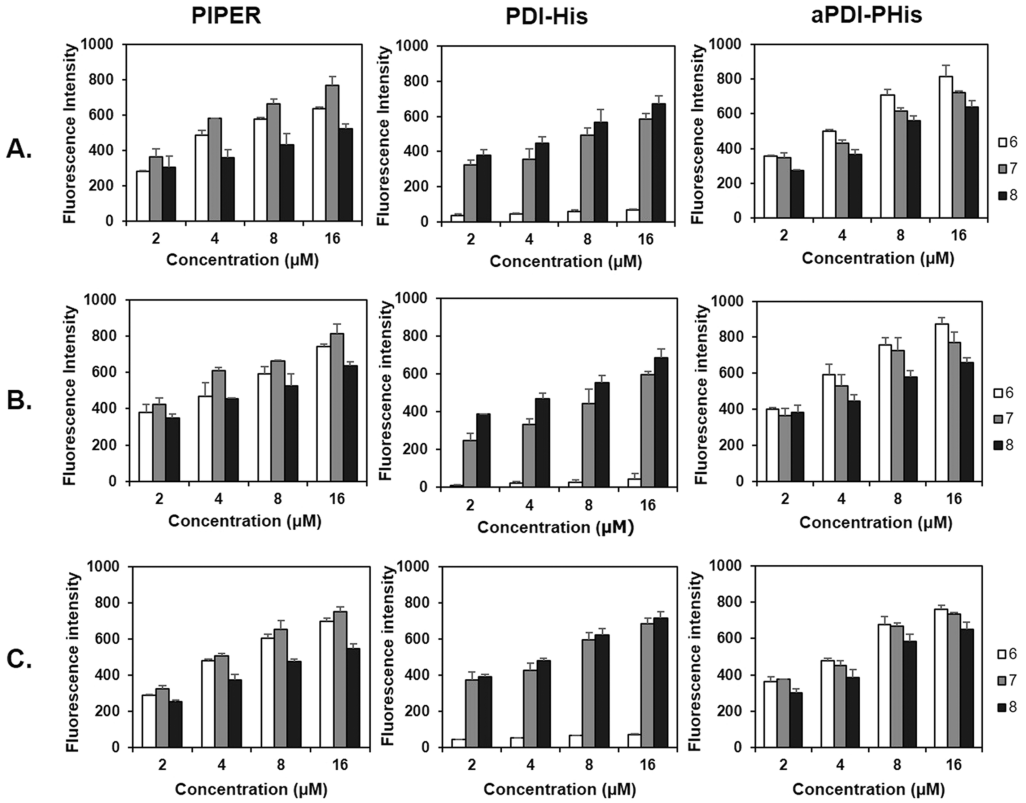

Figure 5. Cellular uptake of the perylenes in PC3 cells (A), LNCaP cells (B), and HEK293 cells (C). The bar graphs represent the mean fluorescence intensity from flow cytometry analysis of the cells after treatment with 0−16 μM concentration of the indicated PDI for 24 h in pH-adjusted culture media.

from the previous octanol/water distribution experiment. It is likely that this compound also aggregates at the interphase of the lipid bilayer and the culture media. Although PIPER is soluble in the order of pH 6 > pH 7 > pH 8, its cellular uptake fails to follow that order; PIPER was uptaken by all three cell lines in the order of pH 7 > pH 6 > pH 8. This trend probably happens because PIPER changes from being lipophilic at pH 7 and 8 to being hydrophilic at pH 6, as indicated by the previous octanol/water distribution experiments. In general, lipophilic compounds are uptaken by cells via passive diffusion better than hydrophilic compounds. Therefore, the lipophilic PIPER at pH 7 is uptaken into the cells better than the more soluble but hydrophilic PIPER at pH 6.

As mentioned earlier, the cancer extracellular microenvironment is mildly acidic. The more cellular uptake in acidic environments but less uptake at normal physiological pH would enhance the benefit of PDI-based anticancer drugs while reducing the unwanted side effects to normal tissues. In this regard, aPDI-PHis might be better poised to tackle cancer cells than PIPER and PDI-His.

DNA Binding Study by Spectrophotometry. Spectrophotometry was employed to observe DNA binding and compound aggregation of our PDIs at pH 6−8. Each PDI (40 μM) was dispersed in 10 mM potassium phosphate buffer (pH 6−8) containing 100 mM KCl in the absence or presence of a preformed DNA structure (20 μM) for 24 h at room temperature. The DNA structures investigated here are two G4 DNAs from the telomeric sequence (Telo-G_4) and the *hTERT* promoter sequence (hTERT-G_4), and a double-stranded (DS) DNA from a 12-mer self-annealed sequence. The visible absorption spectra between 400 and 700 nm were recorded at selected times. Figure 6 shows the absorption spectra of the three PDIs with the preformed DNA structures

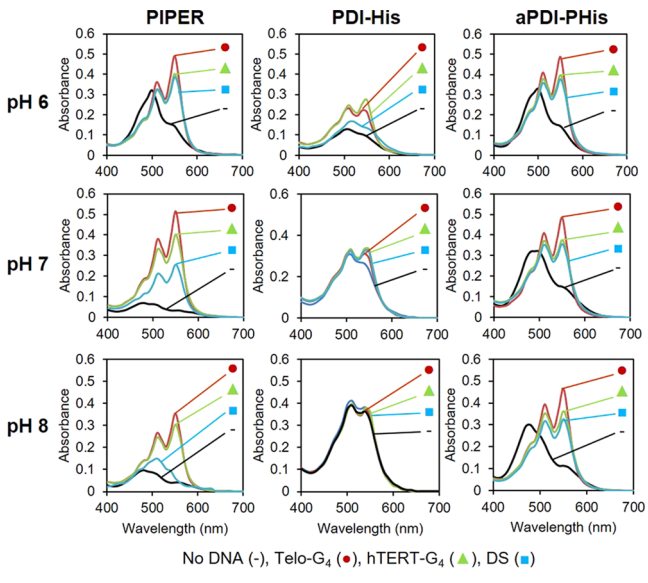

Figure 6. Visible absorption spectra of the perylenes with preformed DNA structures at various pHs. The PDI (40 μM) was dissolved in 10 mM potassium phosphate buffer (pH 6−8) containing 100 mM KCl. Visible wavelengths between 400 and 700 nm were recorded using a UV-1800 double-beam spectrophotometer. The preformed DNA structures are two G-quadruplex DNAs from the telomeric sequence (Telo-G_4) and the *hTERT* promoter sequence (hTERT-G_4), and a double-stranded (DS) DNA from a 12-mer self-annealed sequence.

https://dx.doi.org/10.1021/acsomega.0c03505
ACS Omega 2020, 5, 29733−29745

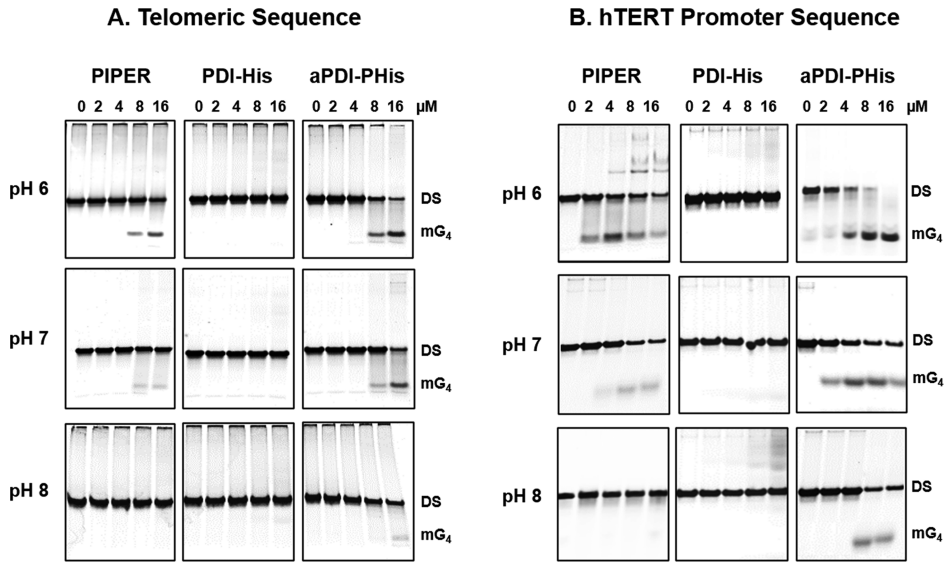

Figure 7. DNA binding selectivity of the perylenes by the duplex−quadruplex competition assay using the telomeric sequence (A) and the *hTERT* promoter sequence (B). The reaction mixture containing the FAM-labeled G-rich strand from the telomeric sequence (A), or the *hTERT* promoter sequence (B), its complementary C-rich strand, and the indicated concentration of the PDI in 10 mM potassium phosphate buffer (pH 6−8) containing 100 mM KCl was incubated at 55 °C for 10 h. The samples were separated by electrophoresis in 16% nondenaturing polyacrylamide gels supplemented with 50 mM KCl. The results were visualized and recorded using a Typhoon phosphoimaging system.

at pH 6−8 after 24 h of incubation. When the PDI binds to a DNA substrate, there is an increase in the absorption intensity and a new absorption maximum at 550 nm. In general, PIPER and aPDI-PHis have the same preference for their DNA substrates in the order of Telo-G_4 > hTERT-G_4 > DS at all three pHs. However, G4 DNAs solubilize PIPER more than duplex DNA at pH 7 and 8, where PIPER aggregates. In other words, G4 DNAs, but not duplex DNA, prevent PIPER from self-aggregation and facilitate its solubility. On the other hand, aPDI-PHis has less self-aggregation at pH 7 and 8, and the soluble molecules can bind to both G4 DNAs and duplex DNA.

The spectra of PDI-His in the absence of a DNA substrate show that the compound aggregates at pH 6 but dissolves at pH 7 and 8. As mentioned earlier, the zwitterionic form of PDI-His side chains at pH 6 reduces its solubility, while the anionic form at pH 7 and 8 enhances its solubility. However, this anionic form of PDI-His has little interaction with any DNA substrates, likely due to the charge−charge repulsion with the sugar−phosphate backbone of DNA. PDI-His shows substrate-dependent interaction only at pH 6, with a preference for G4 DNAs to duplex DNA. The spectra of PDI-His with a G4 DNA show a slight increase in absorption intensity when compared with no DNA substrate. These results suggest that the zwitterionic form of PDI-His at pH 6 reduces its solubility but increases the G4 DNA binding.

DNA Binding Selectivity Study by the Duplex−Quadruplex Competition Assay. Ideally, G4 ligands should bind selectively to G4 DNAs over duplex DNAs to reduce nonspecific toxicity.[32] In our studies, we employed the duplex−quadruplex competition assay to evaluate the ability of our three PDIs for their selective binding to G4 DNAs at pH 6−8. The reaction mixture (2 μM carboxyfluorescein (FAM)-labeled G-rich strand, 2 μM complementary C-rich strand, and the indicated concentration of the PDI in 10 mM potassium phosphate buffer containing 100 mM KCl) was first denatured at 95 °C for 5 min and then incubated at 55 °C for 10 h. The samples were then rapidly cooled to 4 °C before the products were separated by electrophoresis in 16% nondenaturing polyacrylamide gels supplemented with 50 mM KCl. The results were visualized and recorded using a Typhoon phosphoimaging system.

Figure 7A,B shows the results from the duplex−quadruplex competition assay with the telomeric sequence (7A) and the *hTERT* promoter sequence (7B). As illustrated in both figures, both PIPER and aPDI-PHis could selectively induce monomeric G4 (mG_4) formation from both sequences, with a preference toward the *hTERT* promoter sequence over the telomeric sequence. Both compounds also show pH-dependent G4 induction, in which they induced more mG_4 bands at lower pH than at higher pH. When the two compounds are compared, aPDI-PHis induces G4 formation better than PIPER at all three pHs. This result is consistent with the hydrosolubility of both compounds, in which aPDI-PHis dissolves in aqueous solution better than PIPER at neutral pH and basic pH. Moreover, at pH 6, PIPER induced tetrameric G4 and high-MW complexes with the *hTERT* promoter sequence at the higher doses, but not with the telomeric sequence, consistent with the results that we previously published.[12] However, aPDI-PHis induced monomeric G4 (mG_4) with both sequences at all pHs. At 8 μM and above, aPDI-PHis hijacked almost all of the G-rich strand of the *hTERT* promoter sequence to form the mG_4 band at pH 6. Since monomeric G4 induction is more relevant in cellular settings, aPDI-PHis might function better than PIPER. On the contrary, PDI-His seems not to bind to either G4 DNAs or duplex DNA at all three pHs regardless of its hydrosolubility. These results show the importance of the positive charge side chain of PDI for the interaction with G4 DNA.

The above results were obtained with the telomeric and the *hTERT* promoter sequences. However, G4 DNAs can be formed from DNA sequences found in the promoter region of several oncogenes, including *c-Myc*, *VEGF*, *BCL-2*, *c-KIT*, *c-MYB*, *HIF-1α*, *HRAS*, *KRAS*, *PDGF-A*, *PDGFR-β*, *RET*, and

https://dx.doi.org/10.1021/acsomega.0c03505
ACS Omega 2020, 5, 29733−29745

SRC; these sites are potential targets for anticancer therapy by G4 ligands.[33−35] The structural variations of G4 are diverse, and specific G4 ligands can explicitly bind one topology, among others.[34,36] To investigate whether our three PDIs could differentially interact with different G4 DNAs at these three pHs (pH 6−8), we employed a duplex−quadruplex competition assay with two more sequences, the *c-Myc* promoter and *VEGF* promoter sequences. The results are shown in Figure S4, Supporting Information. In general, the results from *c-Myc* and *VEGF* promoter sequences confirmed our results from the telomeric sequence and the *hTERT* promoter sequence, of which PIPER could induce more monomeric G4 (mG_4) at lower pH (pH 6) than at higher pH, while aPDI-PHis could induce monomeric G4 at all three pHs, reflecting their hydrosolubility at those pHs. PDI-His did not induce G4 DNA or bind to duplex DNA from both sequences as well. Interestingly, PIPER had a strong binding preference for the G4 structure from the *VEGF* promoter sequence, while it had a much weaker binding affinity to the G4 structures from the other three sequences. The aPDI-PHis induced monomeric G4 from all four sequences, but it appeared to have a stronger binding preference toward *c-Myc* and *hTERT* promoter sequences than the telomeric and the *VEGF* promoter sequences.

G4 Binding Study by the Fluorescent Intercalator Displacement (FID) Assay. Fluorescent intercalator displacement (FID) assays are used to compare the binding affinity of compounds with various preformed DNA structures; these assays were initially used for identifying DNA duplex binding ligands but have been extended for screening quadruplex-specific ligands.[37−39] To confirm the results from previous experiments, we employed an FID assay to investigate the binding affinity of our PDIs to the G4 structures from telomeric DNA (Telo) and the *hTERT* promoter (hTERT) sequences. Each experiment was performed in a 96-well fluorescence plate. A 0.25 μM preformed DNA target was first mixed with 0.75 μM thiazole orange (TO) in 10 mM potassium phosphate buffer (pH 6−8) containing 100 mM KCl with a total volume of 200 μL. A test compound was then aliquoted into each well stepwise from 0.25 μM to reach the final concentration. At each step, the mixture was allowed to equilibrate for 3 min before the fluorescence recording (λ_{ex} = 501 nm, λ_{em} = 520−700 nm). The percentage of TO displacement was calculated from the formula $100 - [(F_1/F_0) \times 100]$, where F_0 is the initial fluorescence of TO bound to DNA before the addition of compound and F_1 is the fluorescence after the addition of a ligand. The percentage of displacement was then plotted as a function of the ligand concentration. The G4-FID titration plots and TO displacement plots from both sequences are shown in Figures S5 and S6, Supporting Information. The G4-DC_{50} values, which represent the amount of ligand required to displace 50% of bound TO from a G4 target, were determined from the TO displacement plots and are summarized in Table 2.

As shown in Table 2, PIPER binds both G4 structures (from Telo and hTERT sequences) in a pH-dependent manner, with the G4-DC_{50} values in the order of pH 6 < pH 7 < pH 8, and the values are lower with the hTERT sequence than the Telo sequence at all three pHs. These values indicate that PIPER binds the G4 structures at pH 6 better than pH 7 and 8, respectively, and it binds hTERT G4 DNA with higher affinity than Telo G4 DNA. These results support the results from the duplex−quadruplex competition assay, in which PIPER induced the monomeric G-quadruplex at these pHs in the same order. The G4-DC_{50} values of PDI-His exceed the maximum concentration of 2.5 μM at all three pHs, indicating that it binds little to these G4 structures. The results are also similar to the previous duplex−quadruplex competition assay. However, the G4−DC_{50} values of aPDI-PHis are not in the same order as PIPER. It appears that aPDI-PHis binds both G4 structures best at pH 7, with a higher affinity than PIPER at any of the three pHs. The G4−DC_{50} values are also in narrower ranges than PIPER, indicating that aPDI-PHis binds these G4 DNAs more effectively than PIPER within these physiologically relevant pHs. Again, we observed the same trend in the previous duplex−quadruplex competition assay. The FID assay of these PDIs with a duplex DNA yielded DC_{50} values over the maximum concentration of 2.5 μM (data not shown), indicating that these compounds interact very little with duplex DNA.

Table 2. G4-DC_{50} Values of the PDIs to G4 DNAs from Telomeric (Telo) and *hTERT* Promoter (hTERT) Sequences at Three pHs

		G4-DC_{50} value (μM)		
ligand	G4 DNA	pH 6	pH 7	pH 8
PIPER	Telo	0.57 ± 0.12	0.98 ± 0.08	1.85 ± 0.27
	hTERT	0.42 ± 0.28	0.72 ± 0.18	1.48 ± 0.31
PDI-His	Telo	>2.50	>2.50	>2.50
	hTERT	>2.50	>2.50	>2.50
aPDI-PHis	Telo	0.78 ± 0.05	0.28 ± 0.11	0.66 ± 0.14
	hTERT	0.48 ± 0.17	0.36 ± 0.14	0.72 ± 0.25

Altogether, these binding studies show the intricate balance of the effect of both side chains on the hydrosolubility and self-aggregation of the PDIs, and the interaction with DNA structures at various physiologically relevant pHs. When the PDI is less soluble, it either self-aggregates or binds to DNA. There is a preference for G4 formation than duplex formation because the perylene core has a broader $\pi-\pi$ interaction with the G-quartet of G4 than the base-pairing of duplex DNA. The side chains of PDI are equally important; they affect the solubility and the DNA interaction of the PDI. The importance of the cationic side chains on PDIs for DNA binding has been previously observed by us and others.[23,40] Without the cationic side chains, PDI-His fails to bind to either duplex or quadruplex DNA. In the case of aPDI-PHis, it appears that one piperidine side chain is sufficient to bind to G4 DNA, while the histidine side chain facilitates its solubility at the neutral or basic pH. Furthermore, the selectivity of aPDI-PHis toward the monomeric G4 might stem from having only one piperidine side chain, as opposed to two piperidine side chains in PIPER.

Effect of the Perylenes on Telomerase Activity in a Cell-Free System. The G4 ligands facilitate the formation of a G4 structure at the 3′-overhang of telomeres, thereby preventing telomerase from accessing its natural substrate. In this experiment, we investigated our PDIs for their telomerase inhibition in a cell-free system using our fluorescence-based modified telomeric repeat amplification protocol (TRAP) assay.[12] The TSG4 primer was first incubated with various concentrations of a PDI at 37 °C for 2 h in a telomerase reaction mixture (pH 7.4) to allow G4 formation. Then, the crude telomerase extract was added to the mixture, and the telomerase extension reaction was allowed to proceed at 30 °C for another 30 min. After that, the PDI was extracted from the

https://dx.doi.org/10.1021/acsomega.0c03505
ACS Omega 2020, 5, 29733−29745

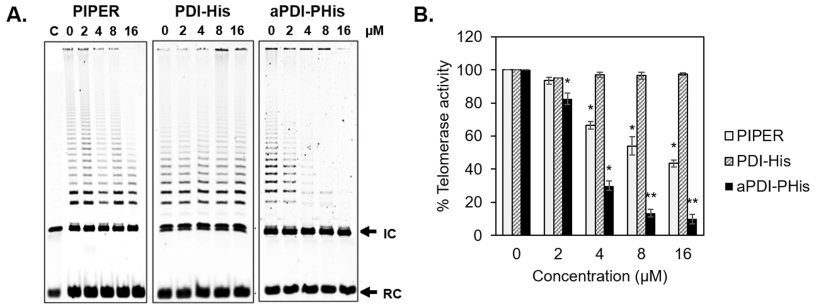

Figure 8. Effect of the perylenes on telomerase activity in a cell-free system: phosphoimages of the TRAP assays (A) and bar graphs representing the results (B). (A) The TSG4 primer was first incubated with the indicated concentration of a PDI at 37 °C for 2 h in a telomerase reaction mixture (pH 7.4) to allow G4 formation. Then, the crude telomerase extract was added to the mixture, and the telomerase extension reaction was allowed at 30 °C for another 30 min. The PDI was removed, and the telomerase products were then amplified by PCR. The amplified products were separated by nondenaturing polyacrylamide gel electrophoresis. IC is the internal control and RC is the recovery control. (B) The bar graph represents the % telomerase activity as a function of PDI concentration. The telomerase activity was determined from the cumulative fluorescence intensity of TRAP products quantified using ImageJ software. Each bar represents the mean telomerase activity ± standard deviation (SD) from three independent experiments. Statistical significance is defined as $*p < 0.05$ and $**p < 0.001$.

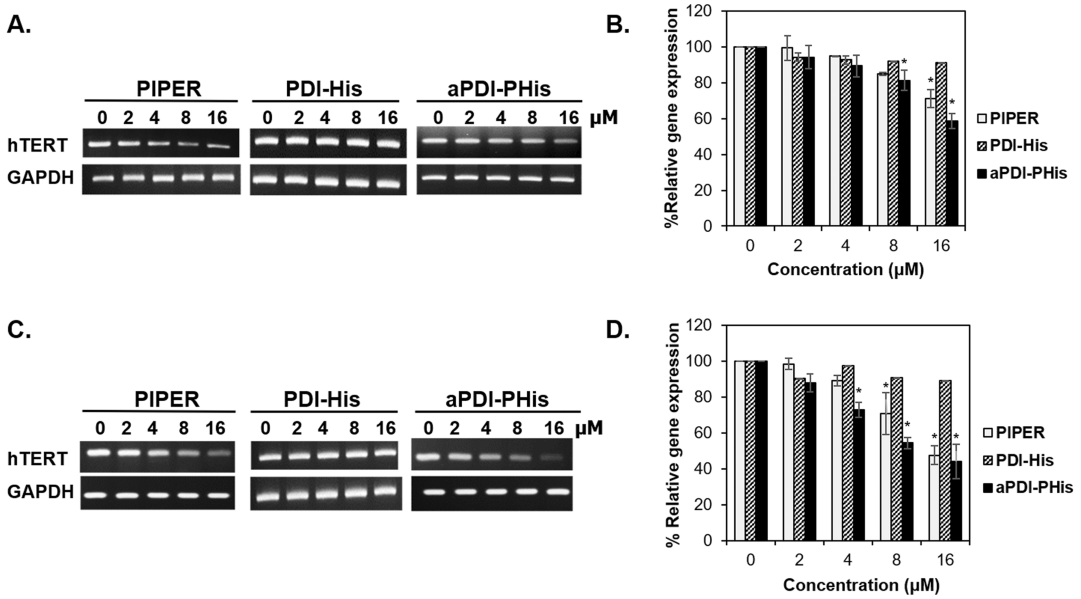

Figure 9. Effect of the perylenes on *hTERT* gene expression: gel images from the RT-PCR assay and bar graphs representing the results in PC3 (A, B) and LNCaP (C, D) cells. (A, C) The cells were treated with the indicated concentration of a PDI for 24 h before their mRNAs were extracted and converted into cDNAs. PCR was then employed to amplify the *hTERT* and *GAPDH* cDNA using specific primers to each cDNA. The PCR products were separated by agarose gel electrophoresis. (B, D) The bar graphs represent the % relative gene expression as a function of PDI concentration in PC3 and LNCaP cells, respectively. Each bar represents the mean relative gene expression ± SD from three independent experiments. Statistical significance is defined as $*p < 0.05$.

reaction mixture by phenol/chloroform extraction, and the telomerase products were precipitated by adding absolute ethanol. The precipitants were resuspended in a polymerase chain reaction (PCR) reaction mixture, and PCR was performed in a thermocycler to amplify the telomerase products. These amplified products were then separated in a nondenaturing polyacrylamide gel electrophoresis (PAGE). The phosphoimages of the TRAP results are shown in Figure 8A, and the bar graphs representing these results from three separate experiments are shown in Figure 8B. As shown in Figure 8A, PIPER and aPDI-PHis inhibited telomerase in a concentration-dependent manner, while PDI-His failed to inhibit telomerase at all concentrations tested. The efficacy of aPDI-PHis is better than that of PIPER, with IC_{50} values of 3.6 ± 0.2 and 8.7 ± 0.4 μM, respectively. The results here are consistent with the G4 binding results from Figure 7A, in which aPDI-PHis bound to the telomeric sequence better than PIPER at pH 7 and 8, while PDI-His did not bind to this sequence at all. These results suggest that PIPER and aPDI-PHis inhibit telomerase through G4 formation at the telomeric sequence.

Acute Cytotoxicity of the Perylenes in Human Prostate Cancer Cells, Peripheral Blood Mononuclear Cells (PBMCs), and HEK293 Cells. Ideal telomerase inhibitors should inhibit telomerase specifically and induce telomere shortening in cancer cells without being toxic to them. In this study, we employed the sulforhodamine B (SRB) assay to evaluate the acute cytotoxicity of our PDIs in two prostate cancer cell lines (PC3 and LNCaP), peripheral blood mononuclear cells (PBMCs), and human embryonic kidney cells (HEK293) following a standard protocol.[41] The cells were treated with various concentrations of a test compound

https://dx.doi.org/10.1021/acsomega.0c03505
ACS Omega 2020, 5, 29733−29745

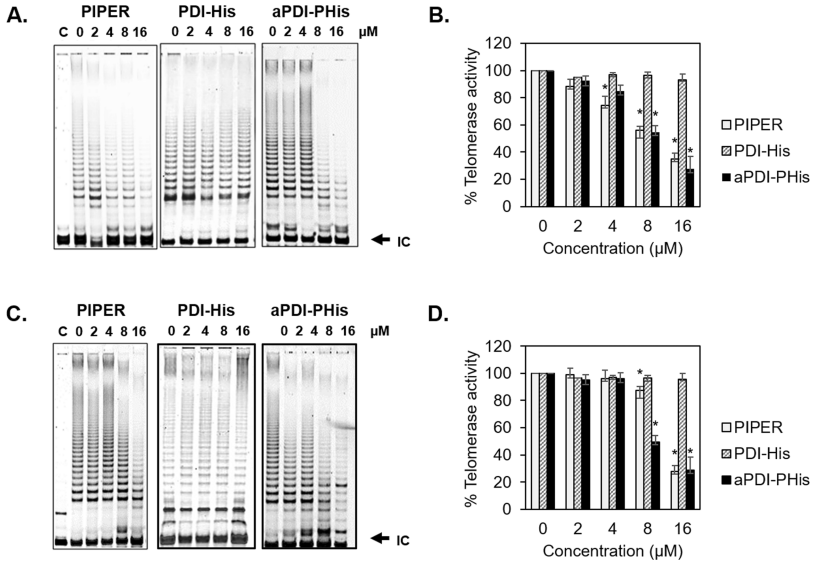

Figure 10. Effect of the perylenes on telomerase activity in prostate cancer cells: phosphoimages of the TRAP assays and bar graphs representing the results in PC3 (A, B) and LNCaP (C, D). (A, C) The cells (5.0×10^5 cells/well) were treated with a test compound for 48 h before they were lysed with CHAPS lysis buffer. A 40 μg sample of protein from the supernatant of the lysed cells served as a source of telomerase in our fluorescent-modified TRAP assay. The products were electrophoretically separated in an 8% nondenaturing acrylamide gel and visualized using a phosphoimaging system. IC is the internal control. (B, D) The bar graphs represent the % telomerase activity as a function of PDI concentration. The telomerase activity was determined from the cumulative fluorescence intensity of TRAP products quantified using ImageJ software. Each bar represents the mean telomerase activity ± SD from three independent experiments. Statistical significance is defined as $^*p < 0.05$.

for 72 h before the cell viability was assayed. The dose–response relationship curves between the compound concentration and the percentage of cell viability were plotted (Figure S7, Supporting Information), and the 50% growth-inhibitory concentration (IC_{50}) values were calculated from these graphs using the software CurveExpert 1.4. The IC_{50} values for PIPER in PC3 and LNCaP cells were 91.5 ± 2.0 and 87.1 ± 4.5 μM, respectively, while the IC_{50} values for aPDI-PHis in PC3 and LNCaP cells were 96.9 ± 3.9 and 95.7 ± 8.4 μM, respectively. The IC_{50} values for PDI-His in both PC3 and LNCaP cells were more than 100 μM, the highest concentration tested in our experiments. Furthermore, all three PDIs showed no reduction in cell viability of PBMC and HEK293 cells at all concentrations up to the maximum of 100 μM (Figure S7C,D). These data show that our PDIs are much less toxic than conventional anticancer drugs.

Effect of the Perylenes on *hTERT* Gene Expression in Prostate Cancer Cells. As mentioned in the Introduction section, G4 ligands facilitate G4 formation at the *hTERT* promoter and suppress its gene expression, resulting in the reduction of hTERT protein, the catalytic subunit of telomerase, and consequently the telomerase activity in cancer cells. Based on our previous publication,[17] PIPER suppressed *hTERT* expression and telomerase activity in PC3 and LNCaP cells with the IC_{50} between 8 and 10 μM. Moreover, a concentration as low as 1 μM of PIPER could induce telomere shortening in the long-term treatment of these cells. Using this knowledge as a guideline, we performed the subsequent cellular experiments using 0–16 μM of the PDIs. In these experiments, we employed a semiquantitative reverse transcription (RT)-PCR analysis to assess gene expression. The cells were incubated with the indicated concentration of a test compound for 24 h before the total mRNAs were extracted. Note that the maximum concentrations of the compounds are much lower than their IC_{50} values for acute cytotoxicity. The RT-PCR was performed to detect the level of gene expression of the *hTERT* and *GAPDH* genes using gene-specific primers. The PCR cycle of each gene was carefully chosen so that the intensity of the detected PCR product was proportional to the initial amount of the cDNA in the reaction. The PCR products were then separated by agarose gel electrophoresis. Figure 9A,C shows the gel results from the PDI-treated PC3 cells and LNCaP cells, respectively. The graphs representing the relative gene expression from three separate experiments are shown in Figure 9B,D. As can be seen in Figure 9A,C, both PIPER and aPDI-PHis suppressed *hTERT* gene expression in a concentration-dependent manner in both PC3 and LNCaP cells, while the housekeeping glyceraldehyde-3-phosphate dehydrogenase (*GAPDH*) gene was not affected. In contrast, PDI-His showed little suppression to the gene when compared to PIPER and PDI-PHis. The aPDI-PHis is slightly more effective than PIPER, as can be seen from the lower percentage of relative gene expression at the same concentration (Figure 9B,D). These results are consistent with the results from the duplex–quadruplex competition assay that we reported earlier, in which aPDI-PHis induced monomeric G4 from the *hTERT* promoter sequence at pH 7 and 8 better than PIPER, and PDI-His could not induce quadruplex formation. These results suggest that the suppression of these gene expressions is through G4 formation at the *hTERT* gene promoter.

Effect of the Perylenes on Telomerase in Prostate Cancer Cells. From the previous experiments, we found that PIPER and aPDI-PHis significantly suppressed *hTERT* gene expression in both PC3 and LNCaP prostate cancer cells. We further investigated whether this suppression of *hTERT* expression would translate to the suppression of telomerase activity in these cells. The cancer cells were treated with the indicated PDI (0–16 μM) for 48 h before their crude cellular contents were extracted and served as the source of telomerase. The same fluorescence-based modified TRAP assay was employed to analyze the telomerase activity from these crude cell extracts. The MTS primer was incubated with the crude

https://dx.doi.org/10.1021/acsomega.0c03505
ACS Omega 2020, 5, 29733–29745

cell extract in a telomerase extension buffer at 30 °C for 30 min. The telomerase-extended products were then directly added into the PCR reaction mixture, and PCR was performed in a thermocycler to amplify the telomerase products. These amplified products were then separated in a nondenaturing PAGE. The phosphoimages of the TRAP results from the PDI-treated PC3 cells and the PDI-treated LNCaP cells are shown in Figure 10A,C, respectively. The bar graphs representing these results from three separate experiments are provided in Figure 10B,D. The results show that PIPER and aPDI-PHis suppress telomerase activity in both cancer cell lines in a concentration-dependent manner, while PDI-His has little to no effect. The IC_{50} values for aPDI-PHis and PIPER in PC3 cells are 9.8 ± 0.4 and 11.3 ± 0.2 μM, respectively, while the IC_{50} values in LNCaP cells are 8.1 ± 0.4 and 10.7 ± 0.4 μM, respectively. The results demonstrate that aPDI-PHis suppresses telomerase activity slightly better than PIPER in both cancer cell lines. These results are consistent with the effect of the PDIs on *hTERT* gene expression described above. Altogether, we conclude that PIPER and aPDI-PHis suppress *hTERT* gene expression through the induction of G4 formation at the *hTERT* promoter, leading to lower functional telomerase and activity in the treated cancer cells.

In conclusion, our studies show that asymmetric PDI can be designed to offer desirable properties and enhanced biological activities. Specifically, by changing one *N*-ethyl piperidine side chain of PIPER to histidine, aPDI-Phis was shown to have better hydrosolubility than PIPER while maintaining its G4 binding and telomerase inhibition. We also found that aPDI-PHis is more soluble and aggregates less in aqueous solution than PIPER at pH 7 and 8. Moreover, while PIPER changes from a lipophilic molecule at pH 7 and 8 to a hydrophilic molecule at pH 6, aPDI-PHis remains lipophilic at all three pHs, which allows aPDI-PHis to diffuse more readily than PIPER into tumors, where the microenvironment is mildly acidic. We also found that aPDI-PHis was uptaken into prostate cancer cells in the order of pH 6 > pH 7 > pH 8, which renders this PDI more effective in tumors and less effective in normal tissues, providing another level of cancer cell selectivity. Moreover, aPDI-PHis was also more effective than PIPER in G4 binding with both the telomeric sequence and the *hTERT* promoter sequence at pH 7 and 8, plausibly because the more soluble aPDI-PHis molecules interact more readily with these DNA sequences. The TRAP assay in the cell-free system at pH 7.4 showed that aPDI-PHis suppresses telomerase activity better than PIPER, reflecting its superior G4 formation at the telomeric sequence. The results from RT-PCR analysis and the TRAP assay from the PDI-treated cells also showed that aPDI-PHis is more effective than PIPER, reflecting its superior G4 formation at the *hTERT* promoter sequence. It appears that having one *N*-ethyl piperidine side chain of the PDI is sufficient for G4 binding since both PIPER and aPDI-PHis can bind G4 DNA, while the negatively charged histidine side chains of PDI-His prevent its interaction. On the whole, these studies warrant the investigation of additional asymmetric PDIs for G4 binding and telomerase inhibition.

METHODS

Materials. All materials were purchased from commercial suppliers and used without further purification. All oligonucleotides and fluorescence-tagged oligonucleotides were supplied by Bio Basic (Canada).

Synthesis of Perylene Derivatives. The syntheses of PIPER, PDI-His, and aPDI-PHis are described in detail in Section S1 (Supporting Information), and the characterization data (^{1}H NMR and MS) of these compounds are shown in Figures S1.1−1.3. The ^{1}H NMR spectra were recorded on a Bruker NEO 400 MHz spectrometer. Mass spectra were recorded on a Thermo LTQ XL instrument.

Visible Absorption Study. The PDI (40 μM) was dissolved in 500 μL of 10 mM potassium phosphate buffer, pH 6−8. The solution was transferred to a quartz cuvette with a 1-cm light path, and the visible wavelengths between 400 and 700 nm were recorded using a UV-1800 double-beam spectrophotometer (Shimadzu Scientific).

Fluorescence Emission Study. The PDI (40 μM) was dissolved in 1 mL of 10 mM potassium phosphate buffer (pH 6−8), and the solution was transferred in triplicate to a 96-well microplate at 200 μL/well. Fluorescence emission spectra were measured using a Synergy H4 hybrid microplate reader (BioTek Instruments, Inc.). The excitation and emission wavelength ranges were set at 480 and 520−700 nm, respectively.

Hydrosolubility Test. The PDI (40 μM) was dissolved in 500 μL of 10 mM potassium phosphate buffer (pH 6−8). The solubility and precipitation of the solution were observed and recorded using a camera at various times up to seven days.

Octanol/Water Distribution Study by the Shake-Flask Method. The general procedure of this experiment was based on OECD Test Guideline 107.[30] The calculation of $\log D_{o/w}$ was based on absorbance measurements of a single liquid phase previously described by Wattanasin et al.[31] The PDI at the indicated concentration was dissolved in buffer-saturated 1-octanol before mixing with 10 mM phosphate buffer at the indicated pH. The bottles were then shaken vigorously for 15 min and centrifuged at 7000*g* for 10 min for phase separation. The concentration of the PDI in the more prominent phase was measured by spectrophotometry.

Cellular Uptake by Flow Cytometry. The PC3 and LNCaP prostate cancer cells (5×10^5 cells) were seeded on a six-well plate in pH-adjusted culture media (Roswell Park Memorial Institute (RPMI) 1640; pH 6−8) for 24 h before they were treated with the indicated concentrations of the PDI for another 24 h, in a humidified 5% CO_2 incubator at 37 °C. The cells were then washed, and the trypsinized cells were collected by centrifuging at 500*g* for 5 min. Cells were then resuspended in 500 mL of phosphate-buffered saline (PBS) before they were analyzed using a CyAn ADP flow cytometer equipped with Kaluza, Flow Cytometry Analysis Software (Beckman Coulter). The data were collected from 50 000 gated events with λ_{ex} of 488 nm and λ_{em} of 680 nm.

DNA Binding Study by Spectrophotometry. The PDI (40 μM) was dispersed in 10 mM potassium phosphate buffer (pH 6−8) containing 100 mM KCl in the absence or presence of an indicated preformed DNA structure (20 μM) for 24 h at room temperature. The visible absorption spectra between 400 and 700 nm were recorded at various times using a UV-1800 double-beam spectrophotometer. The oligonucleotides used in this assay are summarized in Table S1, Supporting Information.

DNA Binding Selectivity Study by the Duplex−Quadruplex Competition Assay. The reaction mixture (2 μM FAM-labeled G-rich strand, 2 μM complementary C-rich strand, and the indicated concentration of the PDI in 10 mM potassium phosphate buffer containing 100 mM KCl) was first

https://dx.doi.org/10.1021/acsomega.0c03505
ACS Omega 2020, 5, 29733−29745

denatured at 95 °C for 5 min and then incubated at 55 °C for 10 h. The samples were then rapidly cooled to 4 °C before the products were separated by electrophoresis in 16% non-denaturing polyacrylamide gels supplemented with 50 mM KCl. The results were visualized and recorded using a Typhoon phosphoimaging system. The oligonucleotides used in this assay are summarized in Table S2, Supporting Information. The telomeric, *hTERT* promoter, *c-Myc* promoter, and *VEGF* promoter sequences are well-characterized G-quadruplex motifs whose G4 structures were verified using NMR.[13,42−46]

Fluorescent Intercalator Displacement (FID) Assay. Each experiment was performed in a 96-well fluorescence plate in 10 mM potassium phosphate buffer (pH 6−8) containing 100 mM KCl, with a total volume of 200 μL. The G4-FID assay was designed as follows: First, 0.25 μM preformed G4 DNA was mixed with 0.75 μM thiazole orange. Then, a test compound was aliquoted into each well stepwise from 0.30 μM to reach the desired concentrations. At each step, the mixture was allowed to equilibrate for 3 min before the fluorescence recording (excitation at 501 nm and emission at 520−700 nm). The $^{G4}DC_{50}$ values, which represent the amount of ligand required to displace 50% of bound TO from a G4 target, were determined by fitting the experimental data using a dose−response curve. The percentage of displacement was calculated from the formula $100 - [(F_1/F_0) \times 100]$, where F_0 is the initial fluorescence of TO bound to DNA before the addition of a compound and F_1 is the fluorescence after the addition of a ligand. The percentage of displacement was then plotted as a function of the concentration of the added ligand. The oligonucleotides used in this assay are summarized in Table S3, Supporting Information.

Telomerase Assay in a Cell-Free System. The effect of the PDIs on telomerase activity in a cell-free system was assayed using our fluorescence-based modified TRAP assay.[11] The TSG4 primer was first incubated with various concentrations of a PDI at 37 °C for 2 h in a telomerase reaction mixture (pH 7.4) to allow G4 formation. Then, the crude telomerase extract was added in the mixture and the telomerase extension reaction was allowed to proceed at 30 °C for another 30 min. After that, the PDI was extracted from the reaction mixture by phenol/chloroform extraction, and the telomerase products were precipitated by absolute ethanol. The precipitants were resuspended in a PCR reaction mixture, and PCR was performed in a thermocycler to amplify the telomerase products. These amplified products were then separated in a nondenaturing polyacrylamide gel electrophoresis (PAGE). The phosphoimages of the TRAP results were visualized and recorded using a Typhoon phosphoimaging system. The oligonucleotides used in the TRAP assay are summarized in Table S4, Supporting Information.

Cell Culture. Prostate cancer cell lines PC-3 (androgen-independent tumor cell lines) and LNCaP (androgen-sensitive carcinoma cell line) were obtained from the American Type Culture Collection. The prostate cancer cell lines were grown in Roswell Park Memorial Institute 1640 (RPMI 1640) with 10% fetal bovine serum (FBS) and 1% antibiotics (50 units/mL penicillin, 50 μg/mL streptomycin). These cancer cell lines were cultured as a monolayer at 37 °C in a humidified atmosphere of 5% CO_2 and 95% air. The peripheral blood mononuclear cells (PBMCs) were collected from healthy volunteers and cultured in the same medium and conditions.

Acute Cytotoxicity Assay. The cell growth inhibition of the PDIs was determined using the sulforhodamine B assay, according to the published protocol.[39] The cancer cells (1.0×10^4 cells) or PBMC cells (1.0×10^5 cells) were incubated with a PDI at 37 °C for 72 h before they were assayed. The 50% growth-inhibitory concentration (IC_{50}) was calculated from the dose−response relationship curve between the drug concentration and the percentage of cell viability using the software CurveExpert 1.4. The reported results represent the mean values of three independent experiments.

Semiquantitative RT-PCR Analysis. The semiquantitative RT-PCR was performed according to our previously published protocol.[10] Briefly, the prostate cancer cells (5.0×10^5 cells) were grown on a six-well tissue culture plate for 24 h before being treated with various concentrations of a PDI for 24 h at 37 °C. The total RNA was collected, and the mRNA was converted into cDNA using the oligo-(dT)18 primer and RevertAid reverse transcriptase (Thermo Scientific). The cDNAs were then amplified by PCR. The PCR cycle of each gene was carefully chosen so that the intensity of the detected PCR product was proportional to the initial amount of cDNA in the reaction. PCR products were then separated by agarose gel electrophoresis and visualized under UV light using a nucleic acid staining solution (RedSafe, Intron Biotechnology). The primer sequences, annealing temperatures, and PCR cycles are summarized in Table S5, Supporting Information.

Telomerase Assay of PDI-Treated Cancer Cells. The telomerase assay of PDI-treated cancer cells was performed according to our previously published protocol.[16] Cancer cells (5.0×10^5 cells/well) were treated with a test compound for 48 h before the cells were lysed with 100 μL CHAPS lysis buffer. Protein (40 μg) from the supernatant of the lysed cells served as a source of telomerase in our fluorescent-modified TRAP assay. The products were electrophoretically separated in an 8% nondenaturing acrylamide gel and visualized using a phosphoimaging system (Typhoon; Molecular Dynamics).

Statistical Analysis. All values are given as mean ± standard derivation (mean ± SD) from three independent experiments. The analysis of variance was performed using the Student *t*-test analysis with SPSS 11.5 software. Differences were considered statistically significant when $*p < 0.05$ and $**p < 0.001$.

■ ASSOCIATED CONTENT

Supporting Information

The Supporting Information is available free of charge at https://pubs.acs.org/doi/10.1021/acsomega.0c03505.

Synthesis and characterization of perylene derivatives; ^{1}H NMR (400 MHz) spectrum and MS data of PIPER; ^{1}H NMR (400 MHz) spectrum and MS data of PDI-His; ^{1}H NMR (400 MHz) spectrum and MS data of aPDI-Phis; percentages of microspecies distribution as a function of pH for PIPER, PDI-His, and aPDI-Phis; fluorescent intensity distributions of the perylenes in prostate cancer cells by flow cytometry; DNA binding selectivity of the perylenes on the *c-Myc* and *VEGF* promoter sequences by the duplex−quadruplex competition assay; G4-FID titration plots of the perylenes on the telomeric sequence and the *hTERT* promoter sequence; TO displacement plots of the perylenes on the telomeric sequence and the *hTERT* promoter sequence; effect of the perylenes on cell viability of

https://dx.doi.org/10.1021/acsomega.0c03505
ACS Omega 2020, 5, 29733−29745

PC3 cells, LNCaP cells, PBMC, and HEK293 cells; oligonucleotides used in the DNA binding study by spectrophotometry (Table S1); oligonucleotides used in the duplex−quadruplex competition assay (Table S2); oligonucleotides used in the fluorescent intercalator displacement (FID) assay (Table S3); oligonucleotides used in the modified fluorescent TRAP assay (Table S4); and primer sequences and conditions used in the semiquantitative RT-PCR studies (Table S5) (PDF)

AUTHOR INFORMATION

Corresponding Author

Wirote Tuntiwechapikul − *Department of Biochemistry, Faculty of Medicine, Chiang Mai University, Chiang Mai 50200, Thailand;* orcid.org/0000-0003-1365-476X; Phone: +66-53-945323; Email: wirotetunti@yahoo.com; Fax: +66-53-894031

Authors

Ratasark Summart − *Department of Biochemistry, Faculty of Medicine, Chiang Mai University, Chiang Mai 50200, Thailand*

Pak Thaichana − *Department of Biochemistry, Faculty of Medicine, Chiang Mai University, Chiang Mai 50200, Thailand*

Jutharat Supan − *Department of Biochemistry, Faculty of Medicine, Chiang Mai University, Chiang Mai 50200, Thailand*

Puttinan Meepowpan − *Department of Chemistry, Faculty of Science, Chiang Mai University, Chiang Mai 50200, Thailand*

T. Randall Lee − *Department of Chemistry and the Texas Center for Superconductivity, University of Houston, Houston, Texas 77204-5003, United States;* orcid.org/0000-0001-9584-8861

Complete contact information is available at: https://pubs.acs.org/10.1021/acsomega.0c03505

Notes

The authors declare no competing financial interest.

ACKNOWLEDGMENTS

This work was supported by grants from (a) the Thailand Research Fund (RSA5880007), (b) the Royal Golden Jubilee Ph.D. (RGJ-Ph.D.) Program (PHD/0198/2556 and PHD/0052/2557), (c) the Faculty of Medicine Research Fund, Chiang Mai University (045/2561 and 095/2561), and (d) the Robert A. Welch Foundation (grant no. E-1320).

REFERENCES

(1) Jafri, M.-A.; Ansari, S.-A.; Alqahtani, M.-H.; Shay, J.-W. Roles of telomeres and telomerase in cancer, and advances in telomerase-targeted therapies. *Genome Med.* **2016**, *8*, No. 69.

(2) Buseman, C.-M.; Wright, W.-E.; Shay, J.-W. Is telomerase a viable target in cancer? *Mutat. Res., Fundam. Mol. Mech. Mutagen.* **2012**, *730*, 90−97.

(3) Crees, Z.; Girard, J.; Rios, Z.; Botting, G.-M.; Harrington, K.; Shearrow, C.; Wojdyla, L.; Stone, A.-L.; Uppada, S.-B.; Devito, J.-T.; Puri, N. Oligonucleotides and G-quadruplex stabilizers: targeting telomeres and telomerase in cancer therapy. *Curr. Pharm. Des.* **2014**, *20*, 6422−6437.

(4) Okamoto, K.; Seimiya, H. Revisiting telomere shortening in cancer. *Cells* **2019**, *8*, No. 107.

(5) Siegel, R.-L.; Miller, K.-D.; Jemal, A. Cancer statistics, 2020. *CA—Cancer J. Clin.* **2020**, *70*, 7−30.

(6) Marian, C.-O.; Wright, W.-E.; Shay, J.-W. The effects of telomerase inhibition on prostate tumor-initiating cells. *Int. J. Cancer* **2010**, *127*, 321−331.

(7) Graham, M.-K.; Meeker, A. Telomeres and telomerase in prostate cancer development and therapy. *Nat. Rev. Urol.* **2017**, *14*, 607−619.

(8) Sklinda, K.; Mruk, B.; Walecki, J. Active surveillance of prostate cancer using multiparametric magnetic resonance imaging: a review of the current role and future perspectives. *Med. Sci. Monit.* **2020**, *26*, No. e920252.

(9) Kim, N. The interplay between G-quadruplex and transcription. *Curr. Med. Chem.* **2019**, *26*, 2898−2917.

(10) Neidle, S. Human telomeric G-quadruplex: the current status of telomeric G-quadruplexes as therapeutic targets in human cancer. *FEBS J.* **2010**, *277*, 1118−1125.

(11) Islam, M.-K.; Jackson, P.-J.; Rahman, K.-M.; Thurston, D.-E. Recent advances in targeting the telomeric G-quadruplex DNA sequence with small molecules as a strategy for anticancer therapies. *Future Med. Chem.* **2016**, *8*, 1259−1290.

(12) Taka, T.; Huang, L.; Wongnoppavich, A.; Tam-Chang, S.-W.; Lee, T.-R.; Tuntiwechapikul, W. Telomere shortening and cell senescence induced by perylene derivatives in A549 human lung cancer cells. *Bioorg. Med. Chem.* **2013**, *21*, 883−890.

(13) Palumbo, S.-L.; Ebbinghaus, S.-W.; Hurley, L.-H. Formation of a unique end-to-end stacked pair of G-quadruplexes in the hTERT core promoter with implications for inhibition of telomerase by G-quadruplex-interactive ligands. *J. Am. Chem. Soc.* **2009**, *131*, 10878−10891.

(14) Riou, J.-F.; Guittat, L.; Mailliet, P.; Laoui, A.; Renou, E.; Petitgenet, O.; Mégnin-Chanet, F.; Hélène, C.; Mergny, J.-L. Cell senescence and telomere shortening induced by a new series of specific G-quadruplex DNA ligands. *Proc. Natl. Acad. Sci. U.S.A.* **2002**, *99*, 2672−2677.

(15) Mancini, J.; Rousseau, P.; Castor, K.-J.; Sleiman, H.-F.; Autexier, C. Platinum(II) phenanthroimidazole G-quadruplex ligand induces selective telomere shortening in A549 cancer cells. *Biochimie* **2016**, *121*, 287−297.

(16) Michelia, E.; D'Ambrosio, D.; Franceschin, M.; Savino, M. Water soluble cationic perylene derivatives as possible telomerase inhibitors: the search for selective G-quadruplex targeting. *Mini Rev. Med. Chem.* **2009**, *9*, 1622−1632.

(17) Kaewtunjai, N.; Summart, R.; Wongnoppavich, A.; Lojanapiwat, B.; Lee, T.-R.; Tuntiwechapikul, W. Telomerase inhibition, telomere shortening, and cellular uptake of the perylene derivatives PM2 and PIPER in prostate cancer cells. *Biol. Pharm. Bull.* **2019**, *42*, 906−914.

(18) Kerwin, S.-M.; Chen, G.; Kern, J.-T.; Thomas, P.-W. Perylene diimide G-quadruplex DNA binding selectivity is mediated by ligand aggregation. *Bioorg. Med. Chem. Lett.* **2002**, *12*, 447−450.

(19) Samudrala, R.; Zhang, X.; Wadkins, R.-M.; Mattern, D.-L. Synthesis of a non-cationic, water-soluble perylenetetracarboxylic diimide and its interactions with G-quadruplex-forming DNA. *Bioorg. Med. Chem.* **2007**, *15*, 186−193.

(20) Franceschin, M.; Pascucci, E.; Alvino, A.; D'Ambrosio, D.; Bianco, A.; Ortaggi, G.; Savino, M. New highly hydrosoluble and not self-aggregated perylene derivatives with three and four polar sidechains as G-quadruplex telomere targeting agents and telomerase inhibitors. *Bioorg. Med. Chem. Lett.* **2007**, *17*, 2515−2522.

(21) Taka, T.; Joonlasak, K.; Huang, L.; Lee, T.-R.; Chang, S.-W.; Tuntiwechapikul, W. Down-regulation of the human VEGF gene expression by perylene monoimide derivatives. *Bioorg. Med. Chem. Lett.* **2012**, *22*, 518−522.

(22) Kato, Y.; Ozawa, S.; Miyamoto, C.; Maehata, Y.; Suzuki, A.; Maeda, T.; Baba, Y. Acidic extracellular microenvironment and cancer. *Cancer Cell. Int.* **2013**, *13*, No. 89.

(23) Tuntiwechapikul, W.; Taka, T.; Béthencourt, M.; Makonkawkeyoon, L.; Lee, T.-R. The influence of pH on the G-

quadruplex binding selectivity of perylene derivatives. *Bioorg. Med. Chem. Lett.* **2006**, *16*, 4120−4126.
(24) Williams, R.-A. Highly soluble asymmetric perylene-bis (dicarboximide)-acceptor system incorporating a methylene bridged methoxybenzene-donor: solvent dependence of charge transfer interactions. *Turk. J. Chem.* **2009**, *33*, 727−737.
(25) Chen, S.; Xue, Z.; Gao, N.; Yang, X.; Zang, L. Perylene diimide-based fluorescent and colorimetric sensors for environmental detection. *Sensors* **2020**, *20*, No. 917.
(26) Dey, S.; Sukul, P.-K. Selective detection of pyrophosphate anions in aqueous medium using aggregation of perylene diimide as a fluorescent probe. *ACS Omega* **2019**, *4*, 16191−16200.
(27) Sun, M.; Müllen, K.; Yin, M. Water-soluble perylenediimides: design concepts and biological applications. *Chem. Soc. Rev.* **2016**, *45*, 1513−1528.
(28) Zhang, E.; Liu, L.; Lv, F.; Wang, S. Design and synthesis of reactive perylene tetracarboxylic diimide derivatives for rapid cell imaging. *ACS Omega* **2018**, *3*, 8691−8696.
(29) Kwon, Y. *Handbook of Essential Pharmacokinetics, Pharmacodynamics, and Drug Metabolism for Industrial Scientists*, 1st ed.; Springer US: New York, 2002; pp 35−72.
(30) *OECD Guideline for the Testing of Chemicals. No. 107: Partition Coefficient (n-Octanol/Water): Shake Flask Method*; OECD Publishing: Paris, 1995.
(31) Wattanasin, P.; Saetear, P.; Wilairat, P.; Nacapricha, D.; Teerasong, S. Zone fluidics for measurement of octanol-water partition coefficient of drugs. *Anal. Chim. Acta* **2015**, *860*, 1−7.
(32) Neidle, S. Human telomeric G-quadruplex: the current status of telomeric G-quadruplexes as therapeutic targets in human cancer. *FEBS J.* **2010**, *277*, 1118−1125.
(33) Balasubramanian, S.; Hurley, L.-H.; Neidle, S. Targeting G-quadruplexes in gene promoters: a novel anticancer strategy? *Nat. Rev. Drug Discovery* **2011**, *10*, 261−275.
(34) Dhamodharan, V.; Pradeepkumar, P.-I. Specific recognition of promoter G-quadruplex DNAs by small molecule ligands and light-up probes. *ACS Chem. Biol.* **2019**, *14*, 2102−2114.
(35) Paul, R.; Das, T.; Debnath, M.; Chauhan, A.; Dash, J. G-quadruplex-binding small molecule induces synthetic lethality in breast cancer cells by inhibiting c-MYC and BCL2 expression. *ChemBioChem* **2020**, *21*, 963−970.
(36) Harikrishna, S.; Kotaru, S.; Pradeepkumar, P.-I. Ligand-induced conformational preorganization of loops of c-MYC G-quadruplex DNA and its implications in structure-specific drug design. *Mol. BioSys* **2017**, *13*, 1458−1468.
(37) Ranjan, N.; Davis, E.; Xue, L.; Arya, D.-P. Dual recognition of the human telomeric G-quadruplex by a neomycin-anthraquinone conjugate. *Chem. Commun.* **2013**, *49*, 5796−5798.
(38) Xing, Y. P.; Liu, C.; Zhou, X.-H.; Shi, H.-C. Label-free detection of kanamycin based on a G-quadruplex DNA aptamer-based fluorescent intercalator displacement assay. *Sci. Rep.* **2015**, *5*, No. 8125.
(39) Mohanty, J.; Barooah, N.; Dhamodharan, V.; Harikrishna, S.; Pradeepkumar, P.-I.; Bhasikuttan, A.-C. Thioflavin T as an efficient inducer and selective fluorescent sensor for the human telomeric G-quadruplex DNA. *J. Am. Chem. Soc.* **2013**, *135*, 367−376.
(40) Franceschin, M.; Lombardo, C.-M.; Pascucci, E.; D'Ambrosio, D.; Micheli, E.; Bianco, A.; Ortaggi, G.; Savino, M. The number and distances of positive charges of polyamine side chains in a series of perylene diimides significantly influence their ability to induce G-quadruplex structures and inhibit human telomerase. *Bioorg. Med. Chem.* **2008**, *16*, 2292−2304.
(41) Vichai, V.; Kirtikara, K. Sulforhodamine B colorimetric assay for cytotoxicity screening. *Nat. Protoc.* **2006**, *1*, 1112−1116.
(42) Bielskutė, S.; Plavec, J.; Podbevšek, P. Impact of oxidative lesions on the human telomeric G-quadruplex. *J. Am. Chem. Soc.* **2019**, *141*, 2594−2603.
(43) Lim, K.-W.; Amrane, S.; Bouaziz, S.; Xu, W.; Mu, Y.; Patel, D.-J.; Luu, K.-N.; Phan, A.-T. Structure of the human telomere in K^+ solution: a stable basket-type G-quadruplex with only two G-tetrad layers. *J. Am. Chem. Soc.* **2009**, *131*, 4301−4309.
(44) Lim, K.-W.; Lacroix, L.; Yue, D.-J.; Lim, J.-K.; Lim, J.-M.; Phan, A.-T. Coexistence of two distinct G-quadruplex conformations in the hTERT promoter. *J. Am. Chem. Soc.* **2010**, *132*, 12331−12342.
(45) Saha, P.; Kumar, Y.-P.; Das, T.; Müller, D.; Bessi, I.; Schwalbe, H.; Dash, J. G-quadruplex-specific cell-permeable guanosine-anthracene conjugate inhibits telomere elongation and induces apoptosis by repressing the c-MYC gene. *Bioconjugate Chem.* **2019**, *30*, 3038−3045.
(46) Sun, D.; Liu, W.-J.; Guo, K.; Rusche, J.-J.; Ebbinghaus, S.; Gokhale, V.; Hurley, L.-H. The proximal promoter region of the human vascular endothelial growth factor gene has a G-quadruplex structure that can be targeted by G-quadruplex-interactive agents. *Mol. Cancer Ther.* **2008**, *7*, 880−889.

https://dx.doi.org/10.1021/acsomega.0c03505
ACS Omega 2020, 5, 29733−29745